RESEARCH PAPER

Channels 8:3, 264–277; May/June 2014; © 2014 Landes Bioscience

Investigating the size and dynamics of voltage-gated sodium channel fenestrations

A molecular dynamics study

Joe A Kaczmarski and Ben Corry*

Research School of Biology; Australian National University; Canberra, ACT Australia

Keywords: Voltage-gated sodium channel, fenestrations, molecular dynamics, ion channel, local anesthetic, Nav1.4, Nav1.2

Abbreviations: BR, bottleneck radius/radii; CHARMM, Chemistry at HARvard Molecular Mechanics; CMAP, cross-term map; DI, DII, DIII, DIV, Domains 1 to 4 (Eukaryotic VGSCs); MD, molecular dynamics; Na+, sodium ions; RCSB, Research Collaboration for Structural Bioinformatics; RMSD, root mean square deviation; S1–S6, alpha helices 1 to 6; SD, standard deviation; SF, selectivity filter; VGSC(s), voltage-gated sodium channel(s); VMD, visual molecular dynamics

Eukaryotic voltage-gated sodium channels (VGSCs) are essential for the initiation and propagation of action potentials in electrically excitable cells, and are important pharmaceutical targets for the treatment of neurological disorders such as epilepsy, cardiac arrhythmias, and chronic pain. Evidence suggests that small, hydrophobic, VGSC-blocking drugs can gain access to binding residues within the central cavity of these channels by passing through lateral, lipid-filled "fenestrations" which run between the exterior of the protein and its central pore. Here, we use molecular dynamics simulations to investigate how the size and shape of fenestrations change over time in several bacterial VGSC models and a homology model of Nav1.4. We show that over the course of the simulations, the size of the fenestrations is primarily influenced by rapid protein motions, such as amino acid side-chain rotation, and highlight that differences between fenestration bottleneck-contributing residues are the primary cause of variations in fenestration size between the 6 bacterial models. In the eukaryotic channel model, 2 fenestrations are wide, but 2 are narrow due to differences in the amino acid sequence in the 4 domains. Lipid molecules are found to influence the size of the fenestrations by protruding acyl chains into the fenestrations and displacing amino acid side-chains. Together, the results suggest that fenestrations provide viable pathways for small, flexible, hydrophobic drugs.

Introduction

Voltage-gated sodium channels (VGSCs) are a class of transmembrane ion channels that regulate the passage of sodium ions (Na^+) across the plasma membrane of a cell. A depolarization of the local membrane potential activates VGSCs toward an open state, allowing the passive influx of Na^+ into the cell through the channel's central pore. As such, eukaryotic VGSCs are crucial for the initiation and propagation of action potentials in neurons and other electrically excitable cells.[1] Mutations in the genes encoding for eukaryotic VGSCs can cause electrical signals to be propagated too often or in an irregular manner, leading to neurological disorders such as epilepsy and cardiac arrhythmias, as well as conditions of chronic and acute pain.[2] Currently, the best treatment for VGSC-related conditions involves the use small organic molecules, such as local anesthetics, which impede the flow of Na^+ through the channels and regulate the rate of electrical signal propagation.[3] However, due to high sequence and structural homology between the 9 subtypes of mammalian sodium channels, drugs which are used to target a specific sodium channel subtype often block the flow of Na^+ through non-target channels, leading to adverse side effects.[4] The development of the next generation of drugs which selectively target certain VGSC subtypes relies on a detailed understanding of how these drugs interact with the channels, and how compounds gain access to the water-filled interior of the channel, where most of the known drug-binding sites occur.[5-8]

The pore-forming α-subunit of eukaryotic VGSCs is a large, single-chained macromolecule which forms a pseudo-tetramer composed of 4 linked homologous domains (DI–DIV).[9] Each domain is made up of 6 α-helices (S1–S6) which form a voltage sensor (S1–S4), and a pore-forming domain (S5–S6). The pore-forming domains of DI–DIV are arranged around the central Na^+-conducting pore of the channel which contains a narrow selectivity filter essential for discriminating between ions,[10] and an "activation" gate at the cytosolic end of the protein that opens and closes the pore in response to changes in the transmembrane potential.[11-13] As a consequence, VGSCs can exist in 3 distinct

*Correspondence to: Ben Corry; Email: ben.corry@anu.edu.au
Submitted: 12/15/2013; Revised: 01/29/2014; Accepted: 02/06/2014; Published Online: 03/14/2014
http://dx.doi.org/10.4161/chan.28136

functional states. In the closed state, the activation gate occludes the central pore and blocks the passage of Na^+ through the channel. In the open state, the activation gate is open and Na^+ can flow unimpeded through the channel. In the inactivated state an additional tethered cytoplasmic loop between DIII and DIV rapidly blocks the cytosolic end of the pore following channel activation, preventing the flow of Na^+.[1]

Most VGSC-blocking drugs bind to residues in the central water-filled cavity of the central pore.[5-8] While it is possible for drugs to reach this site through the activation gate when the channel is open, some neutral drugs are able to block or leave the channel even when it is closed.[14] Given that (1) the size and charge of the selectivity filter prevents access of most drugs via the extracellular side of the pore, (2) charged drugs are unable to yield this so called "tonic block" of resting channels,[5] (3) the channel-inhibiting properties of these compounds diminishes within tens of seconds even in closed-state channels, and (4) the rate of activity loss increases with drug hydrophobicity, this provides evidence for an alternative "hydrophobic" pathway for neutral compounds to reach the interior of the channel.[14] Although use-dependent block is critical to the therapeutic action of many channel-blocking drugs, in this study we focus on the nature of the hydrophobic pathway that is essential for tonic block.

While the general structure of eukaryotic sodium channels is well understood, there are currently no crystal structures available to elucidate the hydrophobic drug entry pathway or to highlight the finer structural details which are needed to guide the development of the next generation of sodium channel-blocking drugs. However, several structures of bacterial VGSCs have been published which can provide a basis for understanding the mechanisms of VGSC-blocking drugs. Bacterial VGSCs—including NaChBac,[15] NavAb,[16] NavMs,[17] and NavRh[18]—share a similar overall architecture to eukaryotic VGSCs but differ in that they are a tetramer consisting of 4 separate homologous subunits.[16] Several bacterial VGSC structures have been published which may highlight the different functional states of the channel. These include the putative pre-open NavAb,[16] inactivated NavAb,[19] open NavMs[17,20] and inactivated NavRh.[18] An interesting feature observed in these structures is the lateral lipid-filled openings, which run between the membrane bilayer and the central pore of the VGSCs (**Fig. 1A**). These "fenestrations" may represent the alternate hydrophobic access pathway for small hydrophobic Na^+-blocking drugs which bind to residues in the central pore of VGSCs. Similar fenestrations were predicted in models made prior to the bacterial structures[21] and have been observed in more recent homology models of eukaryotic VGSCs,[22] and subsequent structural studies on bacterial VGSCs have indicated that the size of the fenestrations may differ between functional states.[17-19] This latter observation led to the suggestion that differences between fenestration sizes could be exploited in the design of drugs which stabilize certain functional states.[17] However, it remains questionable as to whether the differences in fenestration size observed between published crystal structures are caused by changes in the functional state or are simply variations due to sequence differences in the crystallized proteins. These variations could also be an artifact of the static nature of crystallographic structures, which capture only one of many possible protein conformations.

While experimental and computational studies suggest that small, hydrophobic compounds can move through VGSC fenestrations,[22-24] it remains unclear whether larger compounds could traverse these pathways. The ability of drugs to pass through the fenestrations depends on several factors, including the extent of hydrophobic and electrostatic interactions with fenestration-lining residues, but is primarily limited by the size of the fenestrations, and in particular the physical "bottlenecks" that occur within the fenestrations. That physical constrictions in the fenestrations limit drug movement is reinforced by the fact that larger analogs of benzocaine show slower rates of dissociation.[25] The size of the fenestrations in published crystal structures has been compared recently.[26] However, crystal structures only capture a snapshot of the protein and do not show the effect that protein dynamics—ranging from fast side-chain rotations to slower whole-protein movements—or protein–lipid interactions have on the size and shape of the fenestrations. Here, we use molecular dynamics (MD) simulations to investigate the factors that contribute to variations in fenestration size and shape in several bacterial and eukaryotic VGSC models, including the influence of key bottleneck-contributing residues, protein dynamics, the amino acid sequence, and protein–lipid interactions.

Results and Discussion

Bacterial VGSC dynamics and fenestration size

The size and shape of the VGSC fenestrations is likely to be influenced by protein dynamics occurring on a range of time scales. Visual inspection showed that for each bacterial structure the protein remained intact for the whole trajectory and 4 fenestrations could be seen between the S5 and S6 helices of neighboring subunits. Fast vibrational motions of the VGSCs were observed throughout the simulations, including the rapid interconversion between amino acid side-chain rotamers. In each system, backbone RMSD values did not exceed 2.4 Å during the MD simulations (**Fig. S2**), suggesting that the protein structures remained relatively stable. Although the value of the RMSD shows larger fluctuations during periods of the trajectory, consistent with larger conformational changes of the protein, the largest structural motions were observed distant to the fenestrations at the cytosolic end of S5 and terminal end of S6, and there was no clear link between these motions and changes to the fenestration size. Considering that there was limited evidence of larger scale motions in the VGSCs during the simulations, it is likely that fenestration size is primarily influenced by faster motions—such as amino acid side-chain rotations—over the time-course of these simulations.

The size and shape of the fenestrations were analyzed using CAVER, which successfully identified the 4 fenestrations in each of the simulation systems. It also successfully identified tunnels leading out from the central cavity of the protein via the extracellular selectivity filter and via the cytosolic activation gate (**Fig. 1**; **Table S2**); however, these pathways were not analyzed in detail

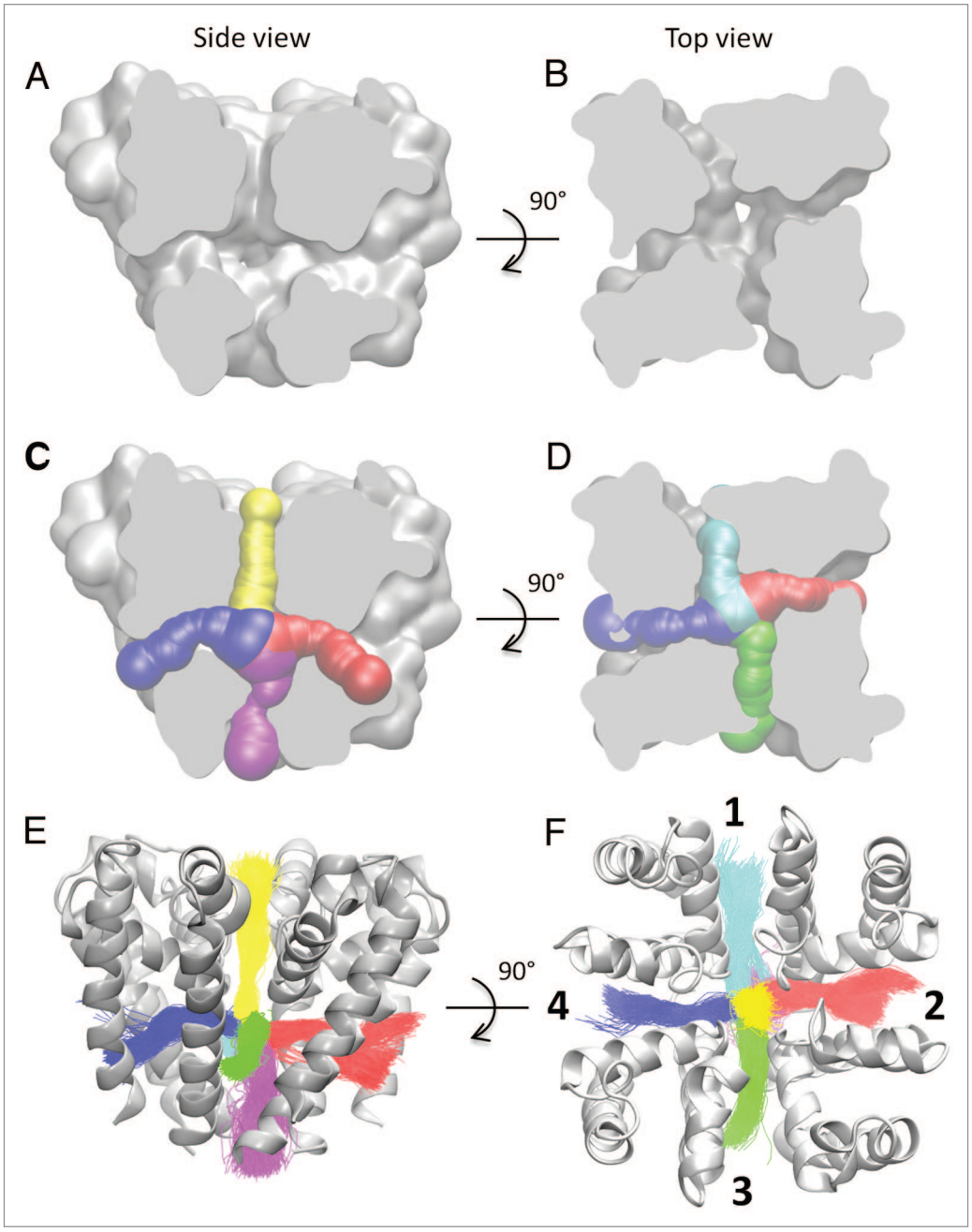

Figure 1. Finding and clustering the fenestrations. A cut through of the protein surface of the NavMs_SYM structure viewed from (**A**) the side and (**B**) the top (extracellular side) shows 2 and 4 fenestrations extending from the central cavity of the channel to the membrane, respectively. In (**A**) the selectivity filter and activation gate are visible at the top and bottom of the structure. Similar views showing the size and shape of the fenestrations found using CAVER are indicated in (**C and D**). The fenestrations found in each snapshot of the simulation trajectory are clustered (**E and F**) to allow for the dimensions of each fenestration to be plotted vs. time. Here, each fenestration cluster is represented by a different color, with each line representing the center of the largest fenestration pathway identified in each snapshot. Each cluster was assigned with a fenestration ID (**F**).

here. In rarer cases, channels leading out from the central cavity to the bulk solvent via other pathways were identified, such as between the S5 and S6 helices of single subunits (data not shown). These tunnels were identified much less frequently and were significantly smaller than the pathways offered by the fenestrations and central pore. Therefore, it is unlikely that these pathways would offer a viable drug access pathway, and so only the 4 primary fenestrations were investigated further.

The average and maximum fenestration bottleneck radii observed in each bacterial VGSC system are outlined in **Table 1** and the distributions of bottleneck radii sampled by the fenestrations during each of the simulations are shown in **Figure 2**. Fenestrations with a minimum radius of at least 0.8 Å were identified in nearly all analyzed frames of the bacterial channel MD simulations. Therefore, it is evident that over the time course of the simulations the fenestrations very rarely, if ever, close up

Table 1. Summary of fenestration properties

Structure	Av. BR (Å)	SD (Å)	Max. BR (Å)
NavAb_CLOSED	1.68	0.32	2.60
NavAb_INACT	1.62	0.35	2.60
NavAb_F203A	1.73	0.27	2.59
NavRh	2.13	0.26	2.83
NavMs	2.11	0.22	2.81
NavMs_SYM	2.20	0.19	2.76

Values for the average and maximum bottleneck radii (BR) for each fenestration as calculated by CAVER. Standard deviations (SD) about the mean are shown for the average bottleneck values. The data from all 4 fenestrations in each structure are pooled in each case. Data for individual fenestrations is given in **Table S2**.

completely. Average bottleneck radii ranged from 1.62 to 2.20 Å and maximum bottleneck radii ranged from 2.59 to 2.83 Å. Some publications have highlighted the possibility that the 4 fenestrations in a given structure may be differentially sized, such as in the inactivated NavAb.[19] However, the results presented here (**Table S2**) suggest that while the sizes of the fenestrations are different at times, there is no consistent difference or symmetry between the size of individual fenestrations within one system. There is no significant difference between the size of the fenestrations in the NavMs and NavMs_SYM systems.

Most sodium channel-blocking drugs contain a phenyl ring[38] and therefore fenestrations need to be wide enough to accommodate these substituents in order to be considered as viable drug-access pathways. The maximum size of the bottleneck radius is

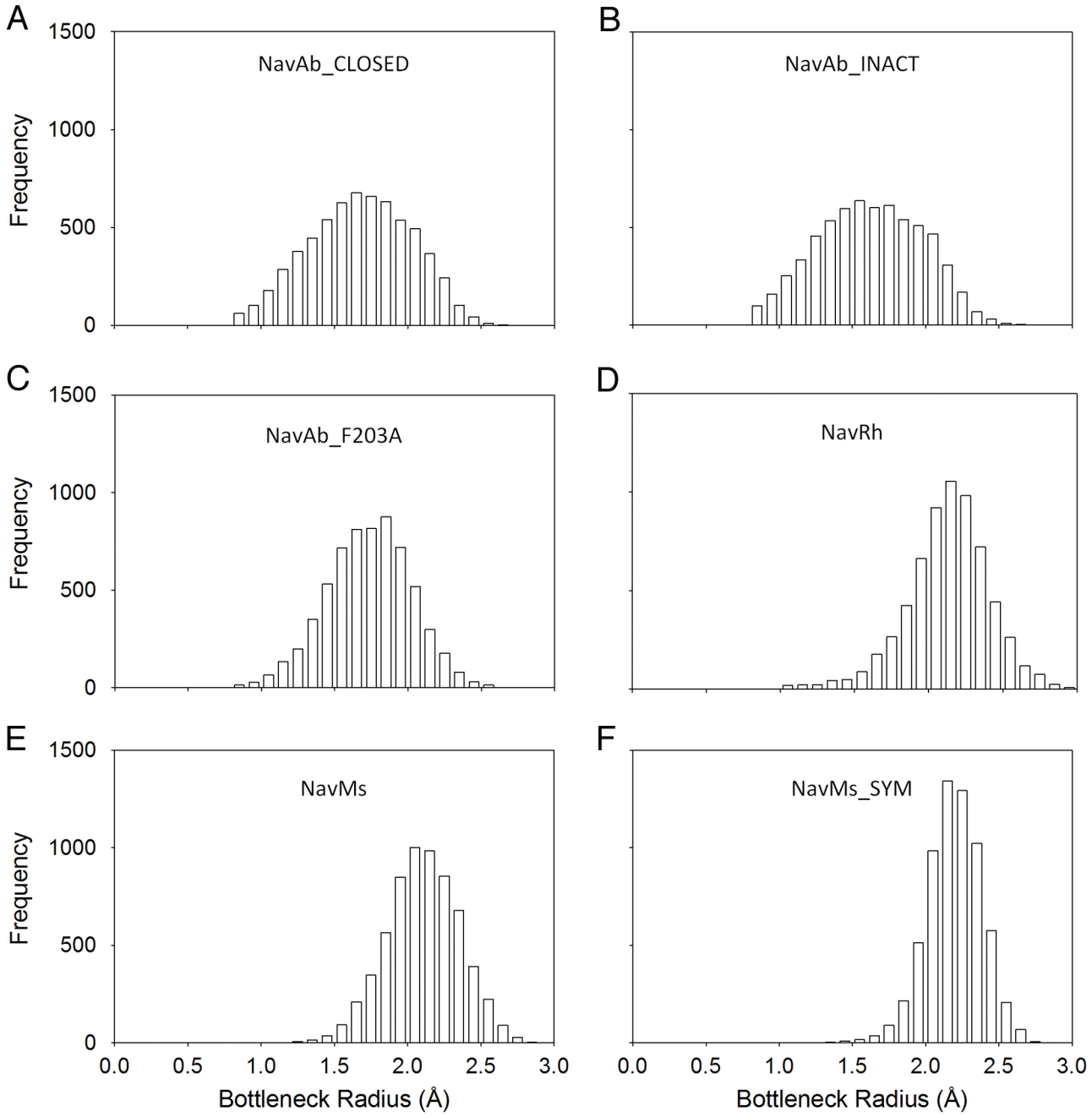

Figure 2 (opposite page). Bottleneck radii distributions. The frequency at which each bottleneck radius is sampled in each system is shown to give an indication of the average fenestration radius and fluctuation in size. Data from all 4 fenestrations in each structure are pooled in each case.

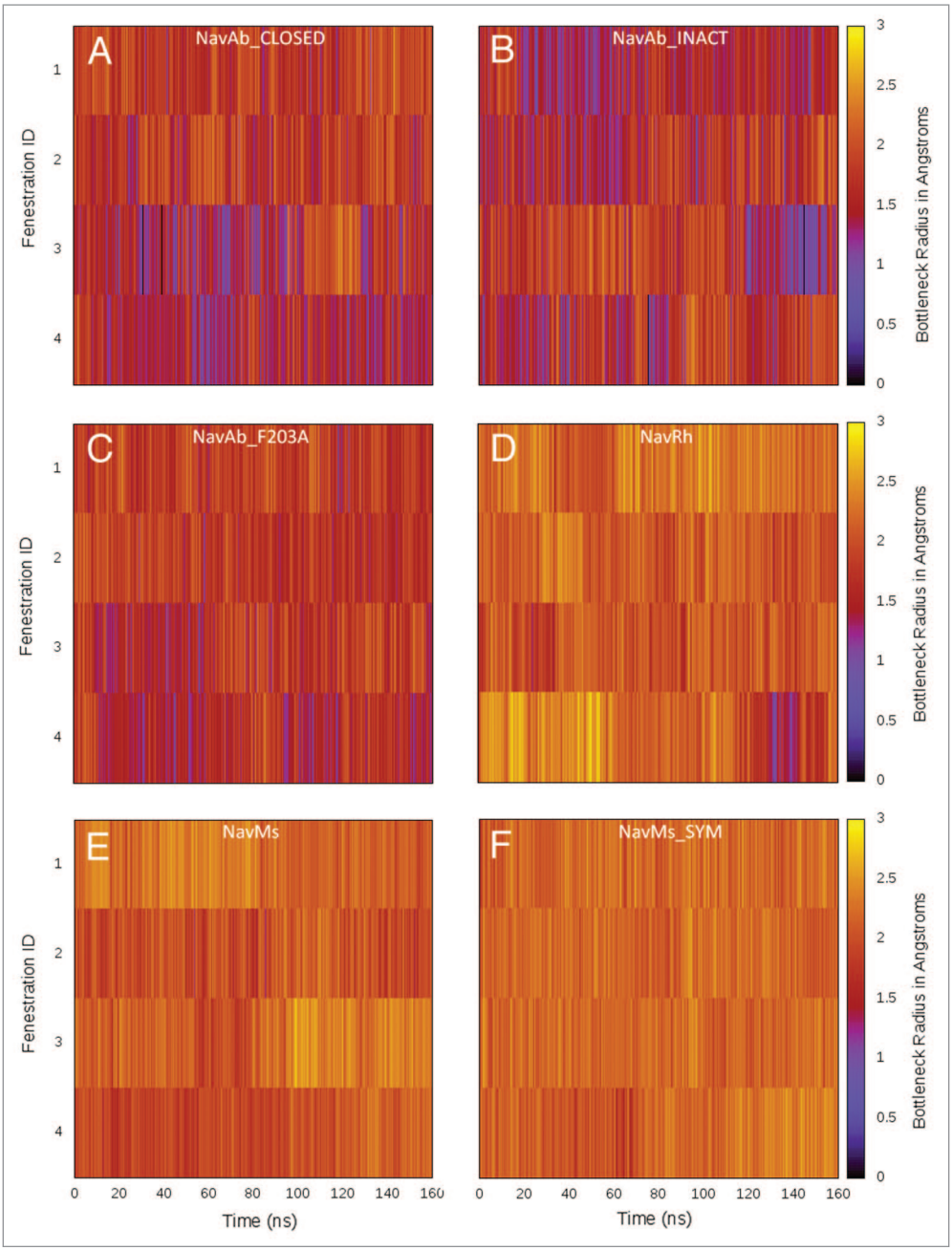

Figure 3. Time evolution of fenestration bottlenecks. The time evolution of the fenestration bottleneck radii (represented by color) are shown for each fenestration in each system.

sufficient for the passage of aromatic rings (diameter ~4.4 Å). The passage of larger drugs through the fenestration may require further distortion of either the protein or the drug. Indeed, a positive correlation between the flexibility of a drug and its ability to pass through VGSC fenestrations has been observed elsewhere,[22] suggesting that the flexibility of compounds should be considered when designing new sodium channel-blocking compounds.

The average and maximum bottleneck radii for the NavAb systems (NavAb_CLOSED, NavAb_INACT, and NavAb_F203A) were significantly smaller and sample a wider range of values than those of the NavRh and NavMs systems. **Figures 3 and 4** show how the bottleneck size and fenestration profiles change over the course of the simulations, respectively. Again, these highlight the more restricted nature of the NavAb_CLOSED, NavAb_INACT, and NavAb_F203A systems. It can be seen

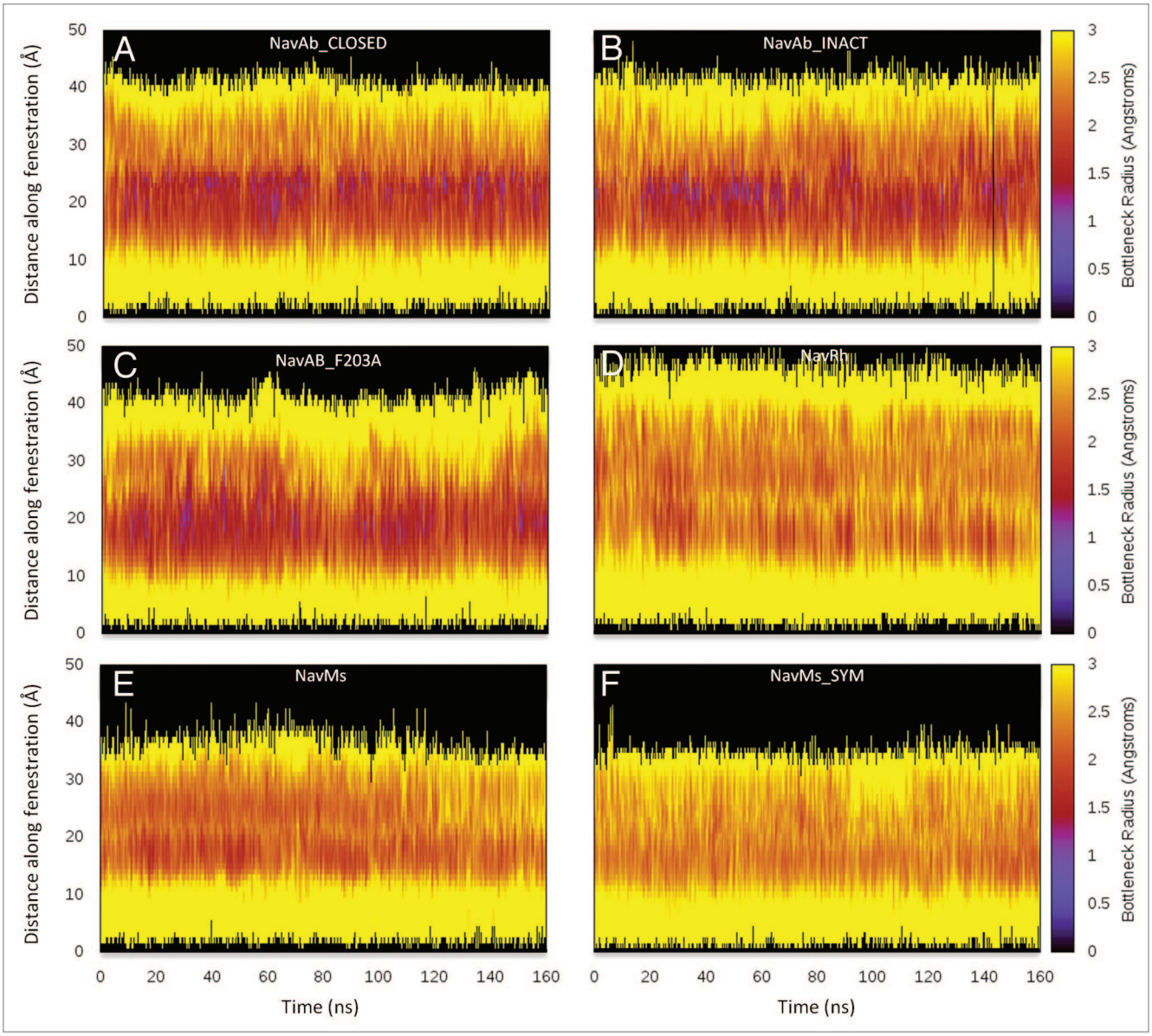

Figure 4. Time evolution of fenestration radius profiles. The time evolution of the profile of one representative fenestration of each system is shown. Distances along the length of the fenestration are given on the y-axis and the width at each position is indicated by the color.

from **Figures 3 and 4** that fenestrations tend to go through periods of a few nanoseconds where they become more restricted, suggesting that protein dynamics on the nanosecond scale are influencing fenestration size.

Highlighting key fenestration bottleneck residues in bacterial VGSCs

While it has been suggested that the size of VGSCs fenestrations may change between functional states, it is likely that amino acid differences between NavAb, NavRh, and NavMs contribute to the differences in fenestration size between these simulations. In order to investigate this in more detail, the residues contributing to the fenestration bottlenecks were identified. Representative heat maps showing the time evolution of fenestration profiles (**Fig. 4**) highlight that bottlenecks occur around halfway along the length of the fenestration. The typical position of the bottleneck is also highlighted in **Figure 5A and B**, which shows the profiles of a single fenestration occurring in 2 snapshots of the NavAb_CLOSED simulation along with the residues contributing to the fenestration bottleneck. Key bottleneck-contributing residues in each system are shown in **Figure 5C**.

In the NavAb_CLOSED and NavAb_INACT structures, 5 key residues act together to create the fenestration bottleneck: M174, T175, F203, T206, and M209. These key bottleneck residues lie in S6 and the P-loop region. The Thr and Met residues encircle the fenestration, and movement of their side-chains restricts and widens the pathway. F203 appears to act as a key gating residue of the fenestrations, lying on S6 near the external mouth of the fenestrations. Attention has been given to this residue in previous studies, since crystal structures capture it in a position in which it blocks the pore of the fenestration.[16,19] Here,

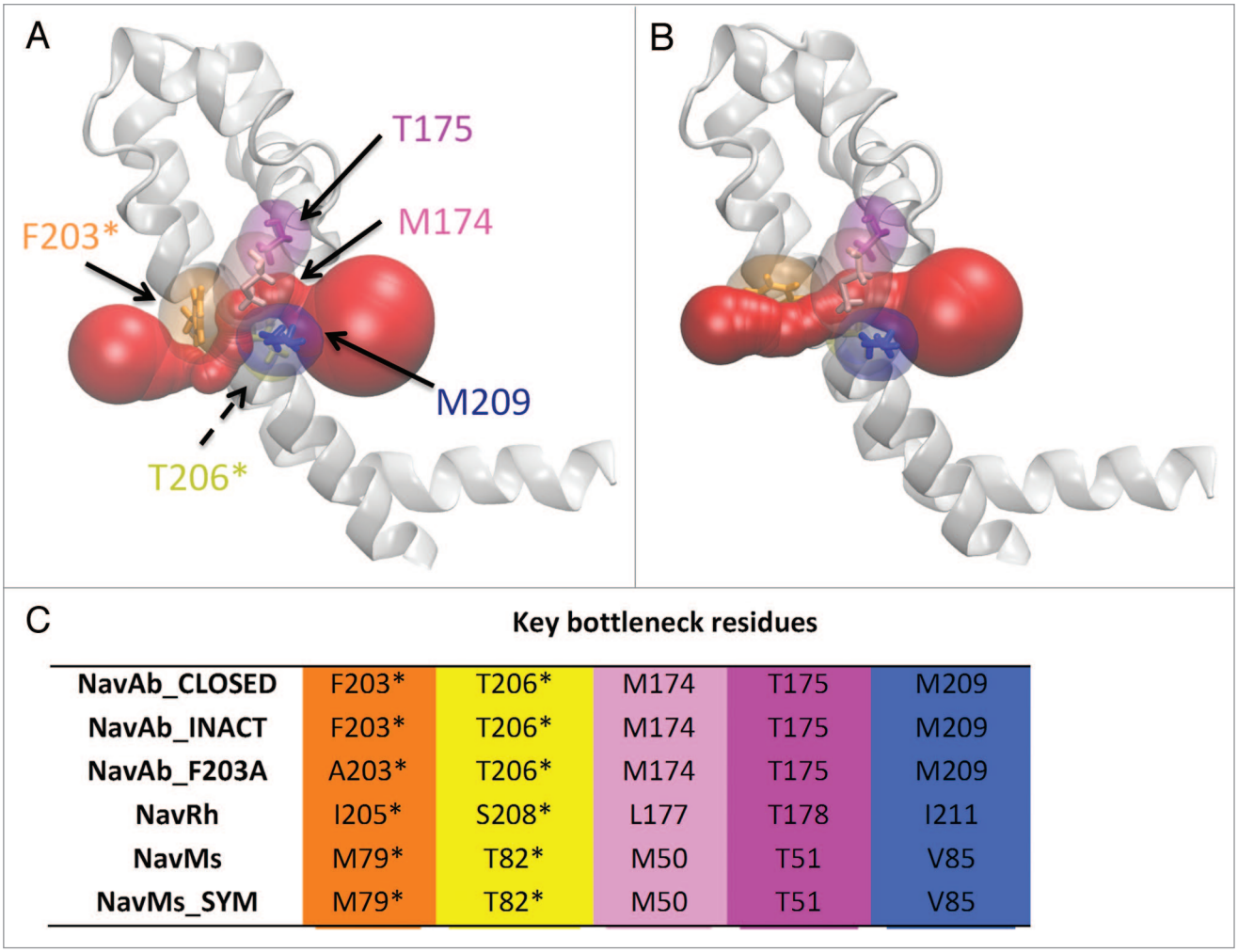

NavAb_CLOSED	F203*	T206*	M174	T175	M209
NavAb_INACT	F203*	T206*	M174	T175	M209
NavAb_F203A	A203*	T206*	M174	T175	M209
NavRh	I205*	S208*	L177	T178	I211
NavMs	M79*	T82*	M50	T51	V85
NavMs_SYM	M79*	T82*	M50	T51	V85

Figure 5. Key bottleneck residues in bacterial VGSCs. The residues lining the fenestration bottleneck in NavAb are shown. Rotation of F203 results in (**A**) a "closed" conformation and (**B**) a more "open" fenestration. The red surface shows the volume of the fenestration found using CAVER and the backbone of one subunit is shown. Asterisked (*) residues come from the subunit shown. The central cavity of the channel is indicated by the large red volume on the right side of each picture and the external entrance of the fenestration is on the left. (**C**) The key bottleneck residues in each of the bacterial structures are shown, aligned according to their sequence position.

we observe that the largest pathways identified by CAVER pass underneath F203, and that rotation of the phenyl ring dramatically changes the shape of the fenestration. When the plane of the phenyl ring lies in line with the fenestrations, the external mouth of the fenestration is reasonably wide (**Fig. 5B**; **Fig. S4A**). When the phenyl ring rotates so that it lies perpendicular to the plane of the fenestrations, the mouth of the fenestration is blocked, the bottleneck of the fenestration restricts, and the main pathway defined by the fenestration becomes more bent (**Fig. 5A**; **Fig. S4B**). Rotation of the phenyl ring occurs rapidly and frequently throughout the simulations, consistent with the pattern of fenestration restriction seen in **Figures 3 and 4**. Occasionally, larger movements completely change the position of F203 moving it toward the bottom of the fenestration mouth (**Fig. S4C**).

The NavAb_F203A mutant shows wider and straighter fenestrations (**Fig. S4D**) compared with the NavAb_CLOSED and NavAb_INACT structures due to the loss of the bulky Phe residue. However, a bottleneck near the Thr and Met residues is still present, which is the reason why the average bottleneck radius for this system is not much larger than that of the other NavAb systems (**Table 1**). However, it is likely that the reduced curvature of the fenestration resulting from this mutation would allow drugs to enter and pass through the fenestrations more easily. Indeed, the F203A mutation allows the passage of isoflurane through the fenestrations in MD simulations with a NaChBac homology model.[23] Further, reducing the size of an equivalent gating residue in eukaryotic channels through the I1761A mutation enhances tonic block at a given local anesthetic concentration in eukaryotic VGSCs.[6] Therefore, residues at this position greatly influence the extent to which drugs can enter and pass through the fenestrations.

A structural alignment revealed that the backbone position of key bottleneck residues are well conserved among the NavAb, NavRh, and NavMs structures (**Fig. S3**). Therefore, differences between fenestration sizes are likely due to differences in amino acid side-chains. The NavRh and NavMs structures contain an

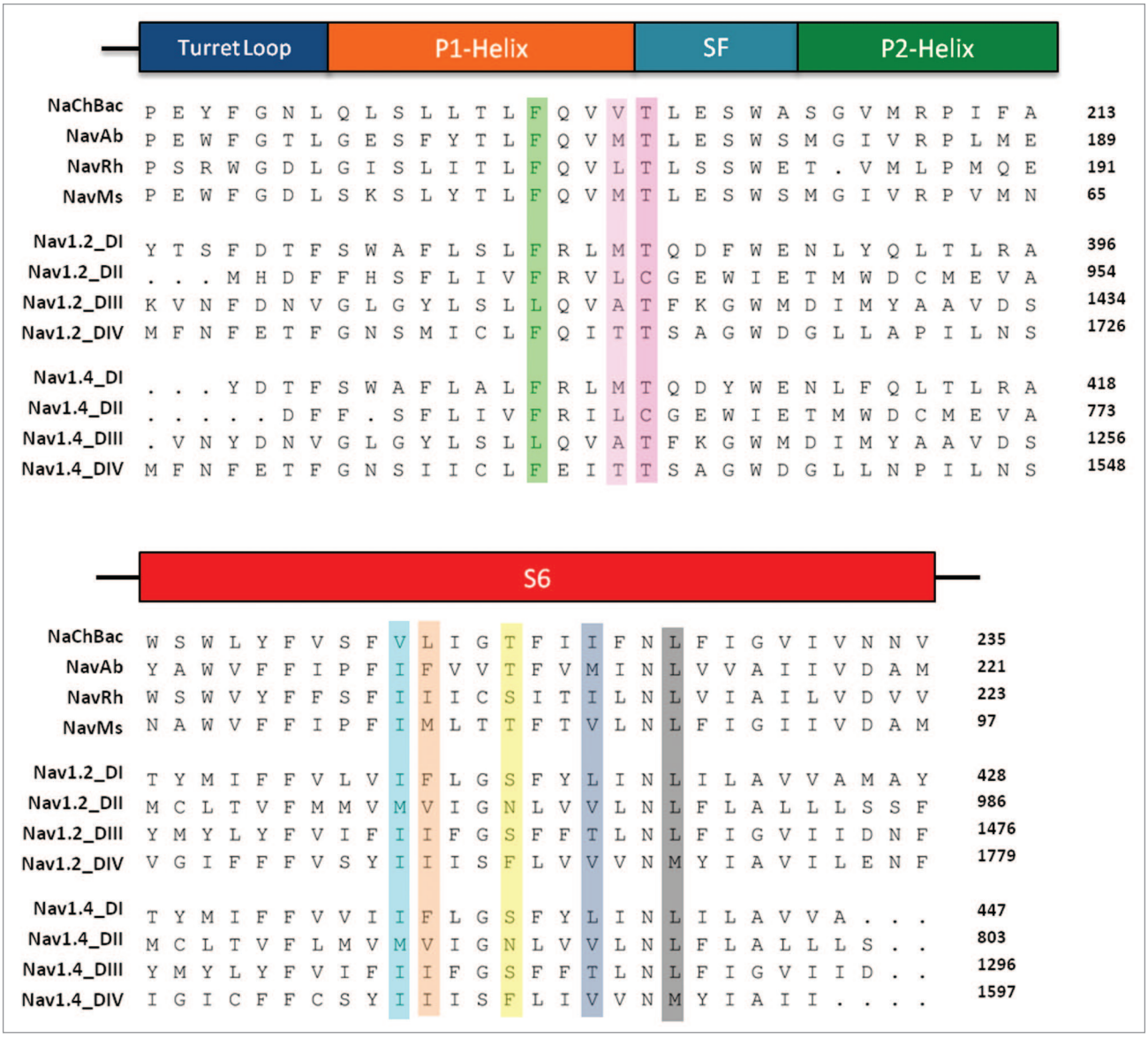

Figure 6. Multiple sequence alignment. A sequence alignment of 4 bacterial VGSCs and the 4 domains of the eukaryotic Nav1.2 and Nav1.4 channels are shown. The positions of key bottleneck residues are highlighted, and colors correspond to those shown in **Figures 5 and 8**. Structural features are shown above the alignment.

Ile and Met in the same position as NavAb's F203, respectively (**Fig. 5C**; **Fig. S4E and F**). Both of these are less bulky than Phe and do not contain an aromatic ring, yielding a wider and straighter fenestration in each of these structures when compared with NavAb. In addition, NavMs also has a shorter Val in the position equivalent to T209 in NavAb while in NavRh a shorter Leu (L177) is in the place of a Met conserved in the NavAb and NavMs structures (M174 and M50, respectively), and a shorter Ser residue (S208) replaces a conserved Thr residue (T206 in NavAb, T82 in NavMs). The presence of these smaller and more flexible bottleneck-contributing residues in NavRh and NavMs contribute to the widening and straightening of the fenestrations compared with the NavAb structures. These sequence differences appear to be more significant than the functional state of the protein in dictating fenestration size.

In addition to the residues previously discussed, several other residues line the fenestrations near the bottleneck region in the bacterial VGSC models. For example, in NavAb F171 acts as a "roof" to the fenestrations near the bottleneck region and I202 is situated near the side wall of the fenestrations. However, these are conserved between NavAb, NavMs, and NavRh channels, and do not appear to contribute to changes in the bottleneck radius as much as the other residues mentioned above.

The fact that some fenestration-lining residues are highly conserved while others vary among VGSCs raises questions about the physiological role of fenestrations. Barber et al.[39] have suggested that fenestrations may simply allow for the flexibility of the pore

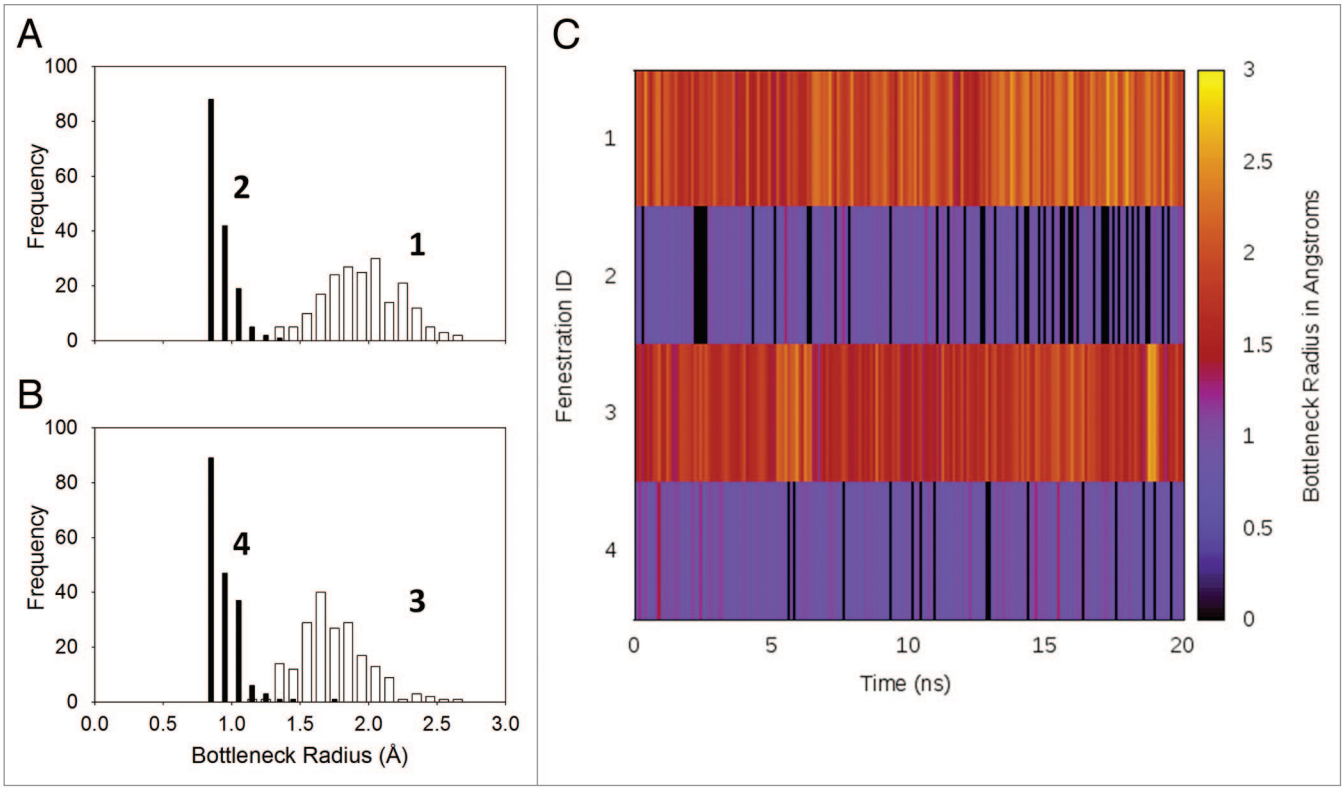

Figure 7. Nav1.4 bottleneck radii distributions and bottleneck heat maps. The frequency at which each bottleneck radius is sampled for each of the 4 fenestrations in Nav1.4 is shown in (**A and B**). Fenestration IDs are labeled. (**C**) The time evolution of the fenestration bottleneck radii are shown for each fenestration in Nav1.4.

domain which is required for gating. Interestingly, while fenestrations seem to be relatively highly conserved among sodium channels, they are less conserved among other ion channels such as potassium channels.[26]

Fenestrations in eukaryotic VGSCs

Are the fenestrations seen in the bacterial VGSC structures also present in eukaryotic channels? If so, could differences in any of the key bottleneck-lining residues be used to design new channel-blocking compounds which specifically target specific VGSC subtypes? Unlike in bacterial channels, the size of individual fenestrations within a single eukaryotic VGSC would be expected to vary significantly due to the heterologous nature of eukaryotic VGSC repeat sequences. Indeed, this has been observed in a recent homology model MD study where hydrophobic drugs were observed to preferentially enter through the wider fenestrations in hNav1.5, a human cardiac VGSC.[22] Several key differences can be noted when the sequences of Nav1.2 (a eukaryotic VGSC expressed in neurons of the central nervous system), and Nav1.4 (a eukaryotic VGSC primarily expressed in skeletal muscle) are aligned with bacterial VGSC sequences (**Fig. 6**). For example, while a Phe residue is found in DI at the position equivalent to NavAb's F203 in both Nav1.2 and Nav1.4, all other repeats have a smaller, non-aromatic residue at this position. The Thr residue equivalent to NavAb's T175 is conserved in 3 of the 4 repeats, but is replaced with a shorter, nucleophilic Cys residue in DII in both eukaryotic channels. Residues in positions equivalent to other key bottleneck-contributing amino acids in bacterial VGSCs vary between DI and DIV. It is likely that the 4 fenestrations in Nav1.2 and Nav1.4 are differentially sized as a consequence of such amino acid differences between the 4 repeats, but since there may be significant structural differences between eukaryotic and bacterial VGSCs, it is difficult to tell if residues at other positions in the sequence contribute to fenestration bottlenecks in eukaryotic VGSCs or if structural differences contribute to a widening or restriction of the fenestrations in other ways.

To gain an appreciation of what the fenestrations might look like in a eukaryotic VGSC, we examined simulations conducted on a homology model of Nav1.4. In **Figure 7A and B** we show the distribution in size of each of the 4 fenestration bottlenecks during a 20 ns simulation. From this, a plot of how the bottleneck radius in each fenestration changes with time (**Fig. 7C**), and a table of the average fenestration radii (**Table S3**), we can immediately see that 2 of the fenestrations are very narrow, while the other 2 have a similar size to those found in the bacterial channels. The size of each fenestration fluctuates with time in a similar manner to that seen in the bacterial channels but the fenestrations between domains DI and DII (Fenestration ID 1), and DIII and DIV (Fenestration ID 3) are always considerably wider than the other 2.

To help understand the reasons for the different fenestration sizes, we show the residues which line the fenestrations of

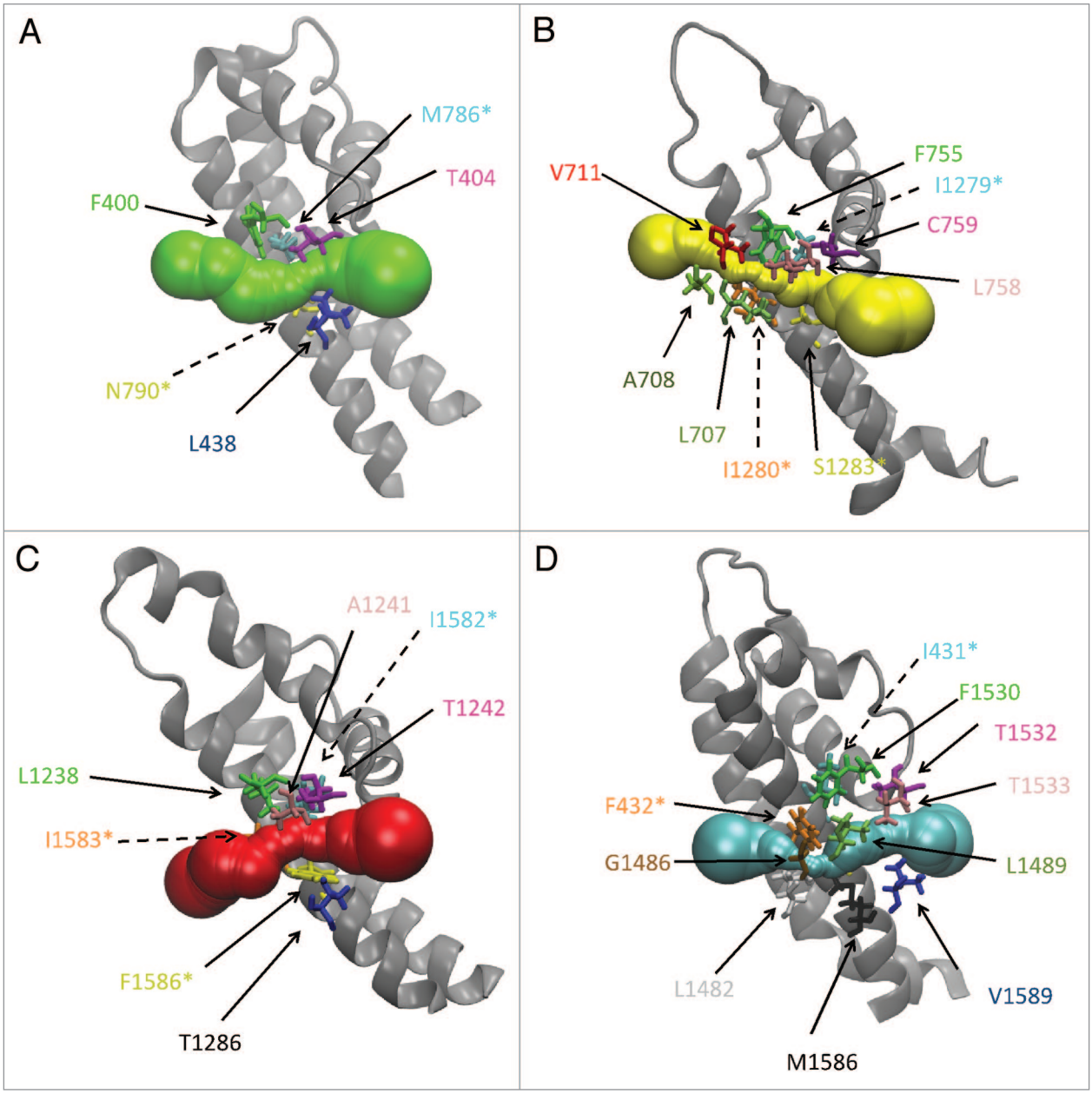

Figure 8. Fenestration lining residues in Nav1.4. A side view of each fenestration in Nav1.4 showing key fenestration-lining residues. Fenestrations corresponding to fenestration IDs 1 (DI–DII), 2 (DII–DIII), 3 (DIII–DIV), and 4 (DIV–DI) are shown in (**A, B, C, and D**), respectively. The volume of the fenestration is shown by the solid surface and the backbone of 1 domain is shown: DII, DIII, DIV, and DI for (**A, B, C, and D**), respectively. Colors of residues correspond to those shown in the sequence alignment (**Fig. 6**; **Fig. S5**).

Nav1.4 in **Figure 8**. In the wider fenestrations—fenestrations 1 (between DI and DII; **Fig. 8A**) and 3 (DIII–DIV; **Fig.8C**)—a small bottleneck occurs about halfway along the fenestration, with bottleneck-contributing residues aligning with those of the bacterial channels (**Fig. 6**). In particular, the main bottleneck of fenestration 1 is encircled by N790, L438, and M786. Movement of the sidechain of M786 has the greatest effect on the fenestration bottleneck size, and correlates with periods of widening and restriction seen in **Figure 7C**. This fenestration has a wide mouth to the lipid bilayer, since the short Val is in place of NavAb's F203 in the gating position. The bottleneck of fenestration 3 is encircled by residues in similar positions (**Fig. 8C**), and has a medium-sized I1583 residue in the gating position. Rotation of residue F1586 has the largest effect on the fenestration size. The mutation of another residue lining this fenestration, I1582A, allows for charged compounds to block the pore when applied externally,[40] but how this change would alter the fenestration size or filter position is not clear.

In contrast, the bottlenecks of the narrower fenestrations 2 and 4 occur closer to the external side of the protein (**Fig. 8B and D**). Unlike fenestrations 1 and 3, the size of these fenestrations is also influenced by residues of S5 (**Fig. S5**). In fenestration 4,

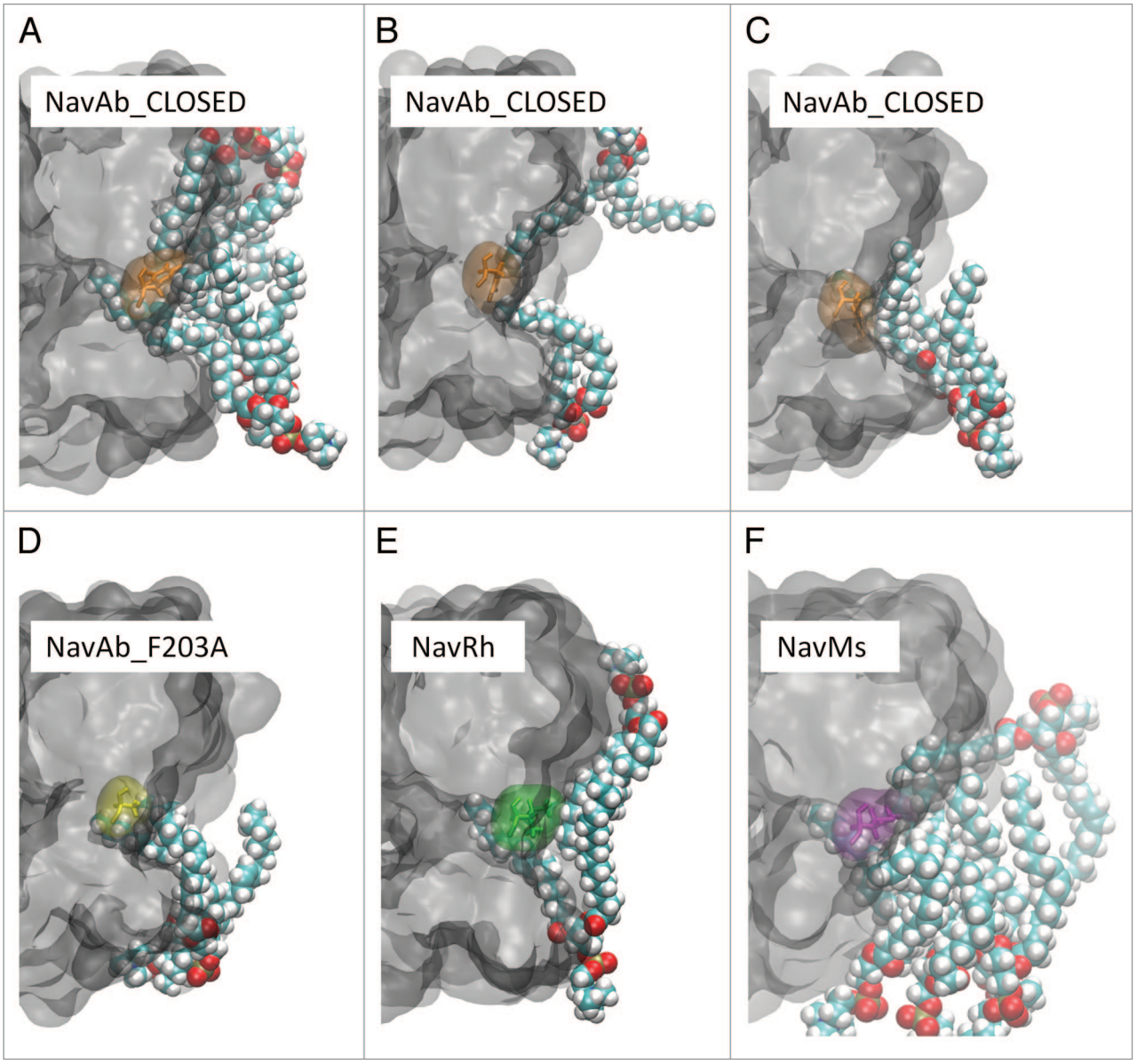

Figure 9. The influence of lipids on fenestration size. (**A–C**) In the NavAb_CLOSED and NavAb_INACT VGSCs, F203 (orange) can prevent lipids from entering the fenestrations. Lipids can more easily extend past gating residues in NavAb_F203A (**D**), NavRh (**E**), and NavMs (**F**).

the gating residue F432 has the most influence on fenestration size. Fenestration 3 is narrow throughout and has I1280 in the position of NavAb's F203. The bulky F755 blocks the fenestration further.

While these results suggest fenestrations 2 and 4 of Nav1.4 would likely be too restricted to act as alternate drug-access pathways, the size of the wider fenestrations 1 and 3 are comparable to those found in NavAb and would be large enough to allow the passage of small compounds. Therefore, mutations in this region would likely affect the passage of such drugs, which would affect tonic block of these VGSCs. The highlighted fenestration contributing residues are conserved between Nav1.2 and Nav1.4, and it is likely that the size of the fenestrations of Nav1.2 is influenced by similar residues. The mutation I1760A in Nav1.2 (equivalent to I1582 in Nav1.4) has been found to enhance tonic block by QX314.[6] Mutation I1761A also affects tonic block in Nav1.2.[6]

The role of lipids in regulating fenestration size

Bacterial VGSC function has been shown to be strongly lipid-dependent;[41] however, most structural and simulation studies have focused solely on the protein. Here, we investigate the effect of lipids on the size of fenestrations. In each simulation, lipid acyl chains ("tails") extended past the gating residues and into the fenestrations for more than 90% of the trajectory, with occasional interchange of lipid molecules, consistent with previous observations.[42] Interestingly, there were clear differences between each of the simulation systems, and the extent to which lipids extended into the fenestration was tightly correlated with fenestration size and the orientation of key bottleneck residues.

In the NavAb_CLOSED and NavAb_INACT systems, lipids extended reasonably far into the fenestrations when the phenyl ring of F203 lay in the plane of the fenestration (**Fig. 9A**). When the phenyl ring lay perpendicular to the fenestration, the lipids did not extend past it (**Fig. 9B**). In some cases, the lipid tail seemed to "trap" the Phe side-chain in certain positions (**Fig. 9C**). In comparison, lipid tails extended much further into the fenestrations in the NavRh and NavMs systems (**Fig. 9D and E**) which lack the Phe gating residue. In the NavAb_F203A system, lipid tails extended past the gating residue more often than in NavAb_CLOSED and NavAb_INACT, but did not extend as far into the fenestration as seen in the NavRh and NavMs systems (**Fig. 9F**), presumably due to the narrowness of the fenestration discussed previously.

There was a clear connection between the presence of lipids in the fenestrations and fenestration size. For example, fenestrations reduced in size when lipids retracted from the fenestrations (compare **Fig. 9A and B**). A widening of the protein fenestration resulting from either conformational changes or amino acid differences would likely make it easier for lipids to enter the fenestration. In turn, the lipid tails were observed to force amino acid side-chains toward the sides of the fenestrations, resulting in a larger pore. In several cases, lipids extended into some, but not all, of the fenestrations in one VGSC at a given time. This corresponded to times when the fenestrations were differentially sized (see **Fig. 3**). The types of lipids found in plasma membranes differs substantially between tissues,[41] and therefore there may be different protein-lipid interactions occurring in different parts of the body. There is scope for future MD studies to investigate how different lipids affect the dynamics of VGSC fenestrations.

Previous simulation studies have shown that lipid tails are displaced when drugs enter the fenestrations.[23] When passing through the fenestrations, it is likely that drugs would need to enlarge the fenestration by displacing side-chains, which are no longer displaced by the lipids. But, since the lipids and hydrophobic drugs would experience similar energetic barriers when passing through the fenestrations, it is likely that the ease of which lipids protrude into the fenestrations reflects how readily drugs could diffuse through the fenestrations.

Methods

Six bacterial VGSC structures were studied: a closed I217C NavAb ("NavAb_CLOSED"), a wild-type putatively inactivated NavAb ("NavAb_INACT"), a F203A mutant of the closed I217C NavAb ("NavAb_F203A"), NavRh ("NavRh") containing a closed activation gate and putatively inactivated selectivity filter, an asymmetric structure of NavMs ("NavMs"), and a symmetrical putatively open model of NavMs ("NavMs_SYM"). The I217C NavAb mutant was used for the NavAb_CLOSED and NavAb_F203A systems rather than the wild-type structure as the crystal structure was solved at a higher resolution.[16] The I217C mutation is situated near the lower part of the activation gate and is unlikely to affect dynamics of the fenestrations. Protein coordinates were obtained from the RCSB Protein Data Bank[27] using the PDB accession codes 3RVY,[16] 4EKW,[19] 4DXW,[18] and 4F4L[17] for the closed NavAb, inactivated NavAb, NavRh, and asymmetric open NavMs, respectively. The symmetrical open NavMs channel, similar to that reported to represent an open channel in McCusker et al.,[17] was produced by creating a tetramer from 4 copies of the most "open" subunits of the 4F4L structure. NavAb_F203A was constructed by introducing the F203A mutation to each of the 4 subunits of the closed NavAb structure using the VMD Mutator Plugin.[28] In each system, the voltage-sensing domain of the VGSC was removed in order to reduce the computational demand of the system. Previous experimental studies have indicated that pore can still represent a functional channel after removal of the voltage sensors.[29,30] No crystallographic waters were included in the initial VGSC structures; however water molecules were able to diffuse into cavities of the protein during equilibration. Ionizable residues were set to their charge configuration at neutral pH in aqueous solution.

Each protein structure was inserted into a pre-equilibrated 1-palmytoyl-2-oleoyl-sn-glycero-3-phosphatidylcholine (POPC) lipid bilayer. A 72 × 72 × 82 Å box of TIP3P water molecules with 250 mM NaCl was used to solvate the system (**Fig. S1**). The system was equilibrated by restraining the α-carbons of the protein while allowing all other atoms in the system to remain unrestrained. The restraint on the α-carbons was defined by a harmonic potential function with a force constant 10 kcal/mol. Once the root mean square deviation (RMSD) values of the protein α-carbons had equilibrated (after 3 ns), the force constant was subsequently reduced to 1 kcal/mol (for an additional 3 ns) and then to 0.1 kcal/mol (for another 3 ns). Following equilibration, each system was simulated unrestrained for 160 ns.

Analysis of a Nav1.4 made use of a homology model and simulation generated by Chen, Robinson, and Chung (personal communication). They constructed the model using NavAb 3RVY as the template and equilibrated the system using similar procedures as described above for the bacterial channels. They ran the system unrestrained for 30 ns prior to 20 ns of data collection.

All simulations were run using NAMD 2.9,[31] the CHARMM27-CMAP force field[32] with torsional cross-terms for the protein, and the CHARMM36 force field[33] for lipids. Ion parameters were taken from Joung and Cheatham.[34] Periodic boundary conditions were used in all simulations, and electrostatic interactions were calculated using the particle mesh Ewald method.[35] Temperature and pressure were kept constant at 298 K and 1 atm, respectively (i.e., an isothermal–isobaric ensemble) using Langevin dynamics and a Langevin piston. A time step of 2 fs was used and bond lengths to hydrogen atoms were kept fixed. The van der Waals cutoff was set to 12 Å. All figures of the simulation system were produced using VMD 1.9.1.[28]

The program CAVER 3.0[36] was used to analyze the size and profile of the fenestrations using aligned structural coordinate (.pdb) files corresponding to every 0.1 ns of the MD simulation. In this program, the outer surface of the protein is calculated by rolling a large spherical probe around the surface of the protein and then internal cavities are identified using a smaller spherical probe (a radius of 0.8 Å was used here). All identified tunnels are grouped into clusters based on relative proximities.

Other parameter values used in CAVER are shown in **Table S1**. The typical clustering of identified tunnel systems is shown in **Figure 1E and F**. As shown in this figure, fenestration clusters were assigned cluster IDs of 1–4, going around the protein in a clockwise manner when looking from the extracellular side of the protein.

A multiple sequence alignment of NaChBac, NavAb, NavMs, NavRh, and the 4 repeats (DI–DIV) of Nav1.2 and Nav1.4 was performed using ClustalW2.[37] All FASTA sequence files were obtained from the RCSB Protein Data Bank.

Conclusion

In this study we have used MD simulations to investigate the factors contributing to the variations in the size and shape of VGSC fenestrations, including the influence of key bottleneck-contributing residues, protein dynamics, and protein–lipid interactions. Results indicate that over the time course of the simulations, changes in fenestration size were primarily caused by fast protein motions such as amino acid side-chain rotations rather than larger conformational changes. Further, key amino acid differences between the NavAb, NavRh, and NavMs channels result in variations in the fenestration size and shape, with gating residues playing a key role in determining the size of the fenestrations. There does not appear to be a clear difference in fenestration size due to channel functional state. Due the computational effort involved, our simulations last only 160 ns each, much shorter than the timescale of the structural changes involved in channel gating and the therapeutic action of local anesthetics. These results do, however, give an indication of the likely size of the fenestrations for a given channel state and whether rapid protein motions will influence the likelihood of drug entry. Furthermore, by comparing the fenestration size in the different crystal structures which are suggested to represent different functional states of the channel it is possible to see that protein conformational changes between these states which take place on a longer timescale are not likely to significantly influence the potential for drugs to move through the lateral fenestrations.

A homology model of the eukaryotic VGSC Nav1.4 has 2 fenestrations that are very narrow and unlikely to be able to allow drugs to pass, but also has 2 fenestrations that are of similar size to those found in the bacterial models. A strong correlation between fenestration size and the presence of lipids which extend into the fenestrations suggest that lipids may play a key role in determining fenestration size, and indicate that drugs would likely need to displace amino acid side-chains in order to pass through the fenestrations.

We hope that highlighting the key residues lining the fenestrations will help to design tests to show if drugs take this route to enter the channel and to help identify sequence difference among the VGSC subtypes that may help to guide the design of the next generation of VGSC-blocking drugs. Although our studies give an indication as to whether compounds can enter the pore via the lateral fenestrations, direct simulation of this process would give a much better appreciation as to what compounds can make use of this pathway, whether specific amino acids lining the fenestrations control the process as well as further elucidating the likely binding sites in the channel. Ultimately the development of subtype selective channel blockers requires a better appreciation as to how well the bacterial homologs can model blockage of human channels and more concrete structural information about the eukaryotic channels. Improved structural information would allow a more in-depth analysis of how the fenestrations differ among the channel subtypes. This information may then be exploited to find compounds that have different rates of passage through the channels and thus display differing abilities to yield tonic block.

Disclosure of Potential Conflicts of Interest

No potential conflicts of interest were disclosed.

Acknowledgments

The authors thank Dr Rong Chen and Dr Shin-Ho Chung for supplying the Nav1.4 homology model and simulation data, and Lewis Martin for helpful advice. This research was undertaken with the assistance of funding from the Australian Research Council (FT130100781) and resources provided at the NCI National Facility systems at the Australian National University through the National Computational Merit Allocation Scheme supported by the Australian Government.

Supplemental Material

Supplemental material may be found here: www.landesbioscience.com/journals/channels/article/28136/

References

1. Vilin YY, Ruben PC. Slow inactivation in voltage-gated sodium channels: molecular substrates and contributions to channelopathies. Cell Biochem Biophys 2001; 35:171-90; PMID:11892790; http://dx.doi.org/10.1385/CBB:35:2:171
2. Ryan DP, Ptácek LJ. Episodic neurological channelopathies. Neuron 2010; 68:282-92; PMID:20955935; http://dx.doi.org/10.1016/j.neuron.2010.10.008
3. Andavan GSB, Lemmens-Gruber R. Voltage-gated sodium channels: mutations, channelopathies and targets. Curr Med Chem 2011; 18:377-97; PMID:21143119; http://dx.doi.org/10.2174/092986711794839133
4. England S, de Groot MJ. Subtype-selective targeting of voltage-gated sodium channels. Br J Pharmacol 2009; 158:1413-25; PMID:19845672; http://dx.doi.org/10.1111/j.1476-5381.2009.00437.x
5. Strichartz GR. The inhibition of sodium currents in myelinated nerve by quaternary derivatives of lidocaine. J Gen Physiol 1973; 62:37-57; PMID:4541340; http://dx.doi.org/10.1085/jgp.62.1.37
6. Ragsdale DS, McPhee JC, Scheuer T, Catterall WA. Molecular determinants of state-dependent block of Na+ channels by local anesthetics. Science 1994; 265:1724-8; PMID:8085162; http://dx.doi.org/10.1126/science.8085162
7. Ragsdale DS, McPhee JC, Scheuer T, Catterall WA. Common molecular determinants of local anesthetic, antiarrhythmic, and anticonvulsant block of voltage-gated Na+ channels. Proc Natl Acad Sci U S A 1996; 93:9270-5; PMID:8799190; http://dx.doi.org/10.1073/pnas.93.17.9270
8. Ahern CA, Eastwood AL, Dougherty DA, Horn R. Electrostatic contributions of aromatic residues in the local anesthetic receptor of voltage-gated sodium channels. Circ Res 2008; 102:86-94; PMID:17967784; http://dx.doi.org/10.1161/CIRCRESAHA.107.160663
9. Noda M, Ikeda T, Suzuki H, Takeshima H, Takahashi T, Kuno M, Numa S. Expression of functional sodium channels from cloned cDNA. Nature 1986; 322:826-8; PMID:2427955; http://dx.doi.org/10.1038/322826a0

10. Corry B. Na(+)/Ca(2+) selectivity in the bacterial voltage-gated sodium channel NavAb. PeerJ 2013; 1:e16; PMID:23638350; http://dx.doi.org/10.7717/peerj.16
11. Blanchet J, Chahine M. Accessibility of four arginine residues on the S4 segment of the *Bacillus halodurans* sodium channel. J Membr Biol 2007; 215:169-80; PMID:17568977; http://dx.doi.org/10.1007/s00232-007-9016-1
12. Blanchet J, Pilote S, Chahine M. Acidic residues on the voltage-sensor domain determine the activation of the NaChBac sodium channel. Biophys J 2007; 92:3513-23; PMID:17325004; http://dx.doi.org/10.1529/biophysj.106.090464
13. Yang N, George AL Jr., Horn R. Molecular basis of charge movement in voltage-gated sodium channels. Neuron 1996; 16:113-22; PMID:8562074; http://dx.doi.org/10.1016/S0896-6273(00)80028-8
14. Hille B. Local anesthetics: hydrophilic and hydrophobic pathways for the drug-receptor reaction. J Gen Physiol 1977; 69:497-515; PMID:300786; http://dx.doi.org/10.1085/jgp.69.4.497
15. Ren D, Navarro B, Xu H, Yue L, Shi Q, Clapham DE. A prokaryotic voltage-gated sodium channel. Science 2001; 294:2372-5; PMID:11743207; http://dx.doi.org/10.1126/science.1065635
16. Payandeh J, Scheuer T, Zheng N, Catterall WA. The crystal structure of a voltage-gated sodium channel. Nature 2011; 475:353-8; PMID:21743477; http://dx.doi.org/10.1038/nature10238
17. McCusker EC, Bagnéris C, Naylor CE, Cole AR, D'Avanzo N, Nichols CG, Wallace BA. Structure of a bacterial voltage-gated sodium channel pore reveals mechanisms of opening and closing. Nat Commun 2012; 3:1102; PMID:23033078; http://dx.doi.org/10.1038/ncomms2077
18. Zhang X, Ren W, DeCaen P, Yan C, Tao X, Tang L, Wang J, Hasegawa K, Kumasaka T, He J, et al. Crystal structure of an orthologue of the NaChBac voltage-gated sodium channel. Nature 2012; 486:130-4; PMID:22678295
19. Payandeh J, Gamal El-Din TM, Scheuer T, Zheng N, Catterall WA. Crystal structure of a voltage-gated sodium channel in two potentially inactivated states. Nature 2012; 486:135-9; PMID:22678296
20. Bagnéris C, Decaen PG, Hall BA, Naylor CE, Clapham DE, Kay CWM, Wallace BA. Role of the C-terminal domain in the structure and function of tetrameric sodium channels. Nat Commun 2013; 4:2465; PMID:24051986; http://dx.doi.org/10.1038/ncomms3465
21. Tikhonov DB, Bruhova I, Zhorov BS. Atomic determinants of state-dependent block of sodium channels by charged local anesthetics and benzocaine. 2006; 580:6027–32.
22. O'Reilly AO, Eberhardt E, Weidner C, Alzheimer C, Wallace BA, Lampert A. Bisphenol A binds to the local anesthetic receptor site to block the human cardiac sodium channel. PLoS One 2012; 7:e41667; PMID:22848561; http://dx.doi.org/10.1371/journal.pone.0041667
23. Raju SG, Barber AF, LeBard DN, Klein ML, Carnevale V. Exploring volatile general anesthetic binding to a closed membrane-bound bacterial voltage-gated sodium channel via computation. PLoS Comput Biol 2013; 9:e1003090; PMID:23785267; http://dx.doi.org/10.1371/journal.pcbi.1003090
24. Lee S, Goodchild SJ, Ahern CA. Local anesthetic inhibition of a bacterial sodium channel. J Gen Physiol 2012; 139:507-16; PMID:22641643; http://dx.doi.org/10.1085/jgp.201210779
25. Quan C, Mok WM, Wang GK. Use-dependent inhibition of Na+ currents by benzocaine homologs. Biophys J 1996; 70:194-201; PMID:8770198; http://dx.doi.org/10.1016/S0006-3495(96)79563-2
26. Corry B, Lee S, Ahern CA. Pharmacological insights and quirks of bacterial sodium channels. In: Ruben P, editor. Voltage Gated Sodium Channels. Springer; 2014.
27. Bernstein FC, Koetzle TF, Williams GJ, Meyer EF Jr., Brice MD, Rodgers JR, Kennard O, Shimanouchi T, Tasumi M. The Protein Data Bank: a computer-based archival file for macromolecular structures. J Mol Biol 1977; 112:535-42; PMID:875032; http://dx.doi.org/10.1016/S0022-2836(77)80200-3
28. Humphrey W, Dalke A, Schulten K. VMD: visual molecular dynamics. J Mol Graph 1996; 14:33-8, 27-8; PMID:8744570; http://dx.doi.org/10.1016/0263-7855(96)00018-5
29. Shaya D, Kreir M, Robbins RA, Wong S, Hammon J, Brüggemann A, Minor DL Jr. Voltage-gated sodium channel (NaV) protein dissection creates a set of functional pore-only proteins. Proc Natl Acad Sci U S A 2011; 108:12313-8; PMID:21746903; http://dx.doi.org/10.1073/pnas.1106811108
30. McCusker EC, D'Avanzo N, Nichols CG, Wallace BA. Simplified bacterial "pore" channel provides insight into the assembly, stability, and structure of sodium channels. J Biol Chem 2011; 286:16386-91; PMID:21454659; http://dx.doi.org/10.1074/jbc.C111.228122
31. Phillips JC, Braun R, Wang W, Gumbart J, Tajkhorshid E, Villa E, Chipot C, Skeel RD, Kalé L, Schulten K. Scalable molecular dynamics with NAMD. J Comput Chem 2005; 26:1781-802; PMID:16222654; http://dx.doi.org/10.1002/jcc.20289
32. MacKerell A, Bashford D. All-Atom Empirical Potential for Molecular Modeling and Dynamics Studies of Proteins. J Phys Chem B 1998; 5647:3586-616; http://dx.doi.org/10.1021/jp973084f
33. Klauda JB, Venable RM, Freites JA, O'Connor JW, Tobias DJ, Mondragon-Ramirez C, Vorobyov I, MacKerell AD Jr., Pastor RW. Update of the CHARMM all-atom additive force field for lipids: validation on six lipid types. J Phys Chem B 2010; 114:7830-43; PMID:20496934; http://dx.doi.org/10.1021/jp101759q
34. Joung IS, Cheatham TE 3rd. Determination of alkali and halide monovalent ion parameters for use in explicitly solvated biomolecular simulations. J Phys Chem B 2008; 112:9020-41; PMID:18593145; http://dx.doi.org/10.1021/jp8001614
35. Essmann U, Perera L, Berkowitz ML, Darden T, Lee H, Pedersen LG. A smooth particle mesh Ewald method. J Chem Phys 1995; 103:8577; http://dx.doi.org/10.1063/1.470117
36. Chovancova E, Pavelka A, Benes P, Strnad O, Brezovsky J, Kozlikova B, Gora A, Sustr V, Klvana M, Medek P, et al. CAVER 3.0: a tool for the analysis of transport pathways in dynamic protein structures. PLoS Comput Biol 2012; 8:e1002708; PMID:23093919; http://dx.doi.org/10.1371/journal.pcbi.1002708
37. Larkin MA, Blackshields G, Brown NP, Chenna R, McGettigan PA, McWilliam H, Valentin F, Wallace IM, Wilm A, Lopez R, et al. Clustal W and Clustal X version 2.0. Bioinformatics 2007; 23:2947-8; PMID:17846036; http://dx.doi.org/10.1093/bioinformatics/btm404
38. Nardi A, Damann N, Hertrampf T, Kless A. Advances in targeting voltage-gated sodium channels with small molecules. ChemMedChem 2012; 7:1712-40; PMID:22945552; http://dx.doi.org/10.1002/cmdc.201200298
39. Barber AF, Carnevale V, Raju SG, Amaral C, Treptow W, Klein ML. Hinge-bending motions in the pore domain of a bacterial voltage-gated sodium channel. Biochim Biophys Acta 2012; 1818:2120-5; PMID:22579978; http://dx.doi.org/10.1016/j.bbamem.2012.05.002
40. Sunami A, Glaaser IW, Fozzard HA. Structural and gating changes of the sodium channel induced by mutation of a residue in the upper third of IVS6, creating an external access path for local anesthetics. Mol Pharmacol 2001; 59:684-91; PMID:11259611
41. D'Avanzo N, McCusker EC, Powl AM, Miles AJ, Nichols CG, Wallace BA. Differential lipid dependence of the function of bacterial sodium channels. PLoS One 2013; 8:e61216; PMID:23579615; http://dx.doi.org/10.1371/journal.pone.0061216
42. Ulmschneider MB, Bagnéris C, McCusker EC, Decaen PG, Delling M, Clapham DE, Ulmschneider JP, Wallace BA. Molecular dynamics of ion transport through the open conformation of a bacterial voltage-gated sodium channel. Proc Natl Acad Sci U S A 2013; 110:6364-9; PMID:23542377; http://dx.doi.org/10.1073/pnas.1214667110